fire

MDPI

Article

New Insight into the Effects of Gaseous CO_2 on Spherically Symmetric Droplet Flames

Ter-Ki Hong [1] and Seul-Hyun Park [2,*]

[1] Department of Mechanical System & Automotive Engineering, Graduate School of Chosun University, 309 Pilmum-daero, Dong-gu, Gwangju 61452, Republic of Korea; tkhong@chosun.ac.kr
[2] Department of Mechanical Engineering, Chosun University, 309 Pilmum-daero, Dong-gu, Gwangju 61452, Republic of Korea
* Correspondence: isaac@chosun.ac.kr; Tel.: +82-62-230-7174; Fax: +82-62-230-7171

Abstract: This study investigated the effect of CO_2 on the burning behavior and radiative properties of a single ethanol droplet flame in microgravity. Measurements of the droplet burning rate, the flame size and temperature, and the radiative emissions were performed, under microgravity conditions for ethanol droplets burning in N_2 and CO_2 environments, using the 1.5 s drop tower facilities at the Korea Maritime and Ocean University (KMOU). The non-monotonic sooting behaviors (caused by the elevated O_2 concentrations) were found to have a significant influence on radiative heat losses in N_2 environments, resulting in non-linear droplet burning behaviors with O_2 concentrations. Due to the unique nature of CO_2 in microgravity, which absorbs radiative energy from the flame and raises the temperatures of the surrounding gases, the CO_2 environments suppressed the radiative heat losses from the flame, regardless of the non-monotonic sooting behavior observed at the higher O_2 concentrations. These experimental findings highlight the complicated physics of CO_2 gas radiation in microgravity, which has not been quantitatively explored.

Keywords: droplet flame; microgravity; radiative heat loss; CO_2 gas

check for updates

Citation: Hong, T.-K.; Park, S.-H. New Insight into the Effects of Gaseous CO_2 on Spherically Symmetric Droplet Flames. *Fire* **2023**, *6*, 461. https://doi.org/10.3390/fire6120461

Academic Editor: Wenjiang Xu

Received: 1 November 2023
Revised: 28 November 2023
Accepted: 30 November 2023
Published: 4 December 2023

1. Introduction

The safety of manned spacecraft for long-term space missions is critical, especially in terms of fire safety. In most terrestrial applications, the use of gaseous CO_2 is well recognized as an effective method of fire suppression [1–5]. Because CO_2 scrubbing systems are required for manned spacecraft or interplanetary habitats, future extraterrestrial fire suppression systems also consider the gaseous CO_2 that is currently used in the ISS fire suppression system [6,7]. Previous investigations [8] on flame spread over solid fuel beds have demonstrated that CO_2 is less effective as a diluent in microgravity than N_2 or He for both thermally thin and thermally thick fuels. In microgravity, the gaseous CO_2 around the flame absorbs radiative energy and thus raises the temperatures of the surrounding gases, which are not convected away due to the absence of buoyant forces, resulting in greater energy feedback to the fuel. In this regard, the radiative feedback effects of CO_2 make it an unsuitable choice as a gaseous fire suppression agent. In a recent computational analysis of cup-burner flames in microgravity, radiative loss was found to be a key loss mechanism in thermal quenching, and the minimum extinguishing concentration (MEC) of the CO_2 environment increased by 32% compared to identical flames in normal gravity [9]. The results of the cup-burner configuration imply that different physicochemical mechanisms exist depending on whether the additional CO_2 is present on the fuel or the oxidizer side of the flame. These findings imply that each of the experimental flame configurations has its own advantages and that a more thorough understanding of the CO_2 radiation impacts in microgravity can be acquired by comparing multiple flame configurations. In this study, a classic droplet configuration [10–13] was employed as a research platform for spacecraft fires to examine the effect of CO_2 on droplet burning.

The influence of ambient CO_2 on droplet flames in microgravity has been investigated experimentally and numerically. Hicks and coworkers [14] reported on the effects of CO_2 around a methanol droplet flame on its burning behavior and its subsequent extinction. They emphasized that ambient CO_2 reduces diffusivity and flame temperature, lowering the burning rate constant, which is clearly observed as a simultaneous reduction in radiative energy output. They also found that larger reductions in the water diffusion coefficient of the methanol droplet flame resulted in a small reduction in the extinction flame diameter. These findings are clearly supported by the subsequent numerical investigations performed by Farouk and Dryer [15]. In their further investigation [16], the effect of ambient CO_2 on droplet flame extinction showed a dramatic transition in the extinction of the larger droplet sizes (>1.5 mm) due to a shift in the extinction mechanism from diffusive to radiative control. Although these investigations contribute to a better understanding of the effects of ambient CO_2 on the burning and extinction of non-sooting methanol droplet flames, which are more affected than other fuels by water absorption, the radiative extinction effects observed in these investigations may differ from those observed in sooting droplet flames.

Recent n-alkane droplet combustion experiments in microgravity onboard the International Space Station (ISS) [17] have shown that increased ambient CO_2 causes a higher fraction of heat loss through radiation compared to heat release, causing the flame temperature to rapidly fall to the critical extinction temperature, which leads to earlier flame extinction. Previous studies [18] have reported that n-alkane fuels exhibit strong sooting tendencies in microgravity. However, the results obtained from the n-alkane droplet combustion experiments carried out onboard the ISS [17] did not account for the significant radiative emissions from the soot formed in the droplet flame. Therefore, the objective of this study is to analyze and provide a comprehensive set of experiments to help elucidate the effect of the radiant emission of CO_2 gas coupled with the sooting behavior of microgravity droplet flames. To this end, a variety of measurements including droplet burning rate, flame temperature, soot-volume fractions, and radiative emissions were performed in microgravity for ethanol droplets burning in N_2 and CO_2 environments. Ethanol was chosen as the droplet fuel for this study because it allows for a broad range of sooting. Previous studies [19] have shown that the burning of ethanol droplets in microgravity produces soot when higher ambient pressure is combined with higher oxygen concentrations. Once sooting begins at the higher flame temperature (afforded by the oxygen concentration variations) and ambient pressure, the observed sooting trends of ethanol are similar to those observed for n-alkane fuels such as n-heptane [20] and n-decane [21].

2. Experimental Descriptions

A series of drop experimental campaigns were carried out using the 1.5 s drop tower facilities (see Figure 1a) at the Korea Maritime and Ocean University (KMOU). The schematic diagram of the experimental drop apparatus is shown in Figure 1b. When the experimental drop apparatus is released from the top of the drop tower facilities, it experiences microgravity for approximately 1.5 s. The experimental drop apparatus illustrated in Figure 1b,c comprises a 12 L combustion chamber with five optical access windows, a diode laser, a beam expander and collimator, high-resolution CCD cameras, and electro-mechanical components on the platform inside the combustion chamber. This platform is designed to take autonomous measurements of several parameters such as the soot-volume fraction, the flame temperature, the flame radiative emission, and the droplet burning rate of an isolated droplet flame in microgravity. Only a brief summary of the experimental drop apparatus and measurement technique are provided here since more information can be obtained elsewhere [22].

(**a**) 1.5 s drop tower facilities at the KMOU

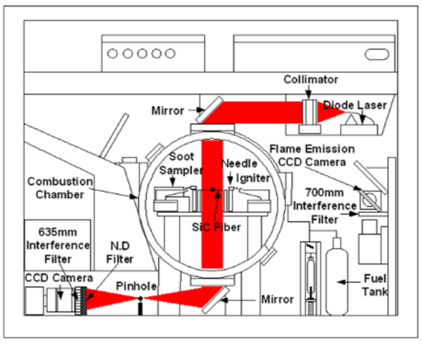

(**b**) Experimental drop aparatus

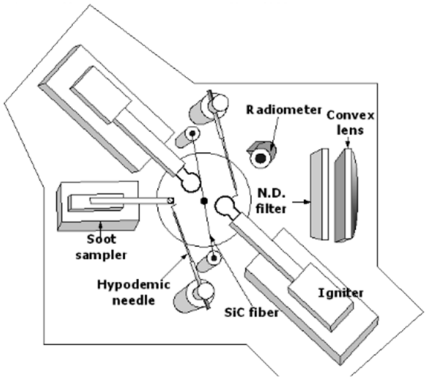

(**c**) Measurement platform

Figure 1. Experimental facilities and apparatus for microgravity droplet combustion.

The liquid ethanol was delivered from a fuel reservoir through two hypodermic needles using a 1.0 mL solenoid-activated syringe (0.25 mm in diameter). The ethanol dispensed from the hypodermic needles formed a droplet on a 15 µm silicon carbide (SiC) filament (which was used to tether the droplet to keep it from moving out of the field of view). Two horizontally opposed hot-wire igniters were used to ignite the liquid droplet during the free fall. The laser-backlit diagnostic equipment for measurements of the droplet burning rate and soot-volume fractions is the most critical component. In this equipment, the laser beam produced using a 635 nm diode laser was expanded to 50 mm in diameter and was then collimated. The expanded and collimated laser beam was redirected through the top optical port. The laser beam passing through the combustion chamber was focused using a 200 mm focal length plano-convex lens fitted to the bottom optical port. The focused laser beam was then reflected toward a high-resolution CCD camera. In front of the CCD camera, a zoom lens with a bandwidth filter for a wavelength of 635 nm was applied to obtain the required magnification for the spatially resolved droplet and the soot-containing region.

To measure the droplet burning rate, the laser-backlit images of the droplet were captured and then digitized frame by frame with high-resolution frame acquisition software. In this study, the droplet burning rate constant K was experimentally determined by measuring the regression of the square of the droplet diameter over time. A full-field light-extinction and tomographic inversion technique was applied to measure the soot-volume fraction distributions within the flame. The projected light-extinction ratio distributions (the transmitted image divided by the incident image) obtained as a function of time were used to determine the soot-volume fraction fv using the three-point Abel deconvolution technique [23]. The radiative emission from the flame was measured using a radiometer which was placed 12.5 cm from the droplet center, as shown in Figure 2. The spectral

response of the radiometer ranges from 1 µm to 20 µm, which covers the majority of the radiation emitted from the broadband via the soot particles and the spectral radiation emitted by the radiating gases, such as CO_2 and H_2O.

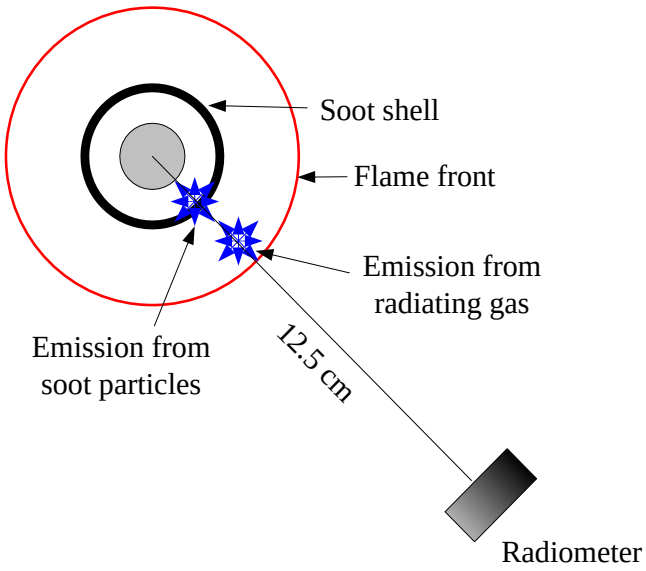

Figure 2. Radiative emission measurements from a single droplet flame.

Thin filament pyrometry (TFP), a method that has been extensively studied in previous studies on laminar diffusion flames [24,25], was used to determine the temperature of the droplet flame. The TFP technique involves measuring the radiation intensity from the SiC filament (the same filament used to tether the droplet) and determining the temperature of the measured gray-body emission from the SiC filament using the Planck equation. The emission from the SiC filament at 700 nm imaged using the high-resolution CCD camera is shown in Figure 3a. Flame radii were determined by measuring the spatial extent of the maximum luminosity region of the SiC filament (see Figure 3b).

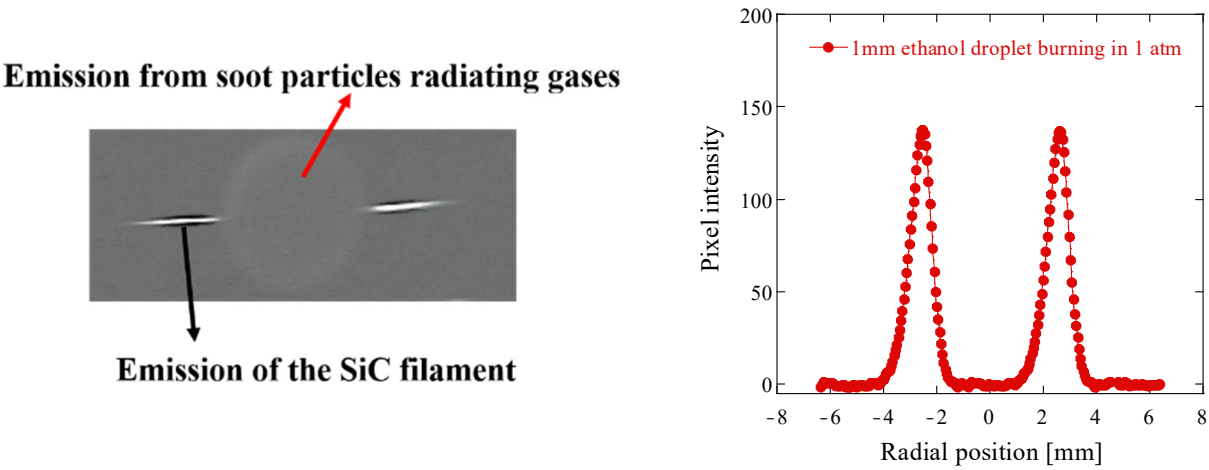

(**a**) Gray-body emissions from the flame and the SiC filament (**b**) Spatially resolved emission intensity from the SiC filament

Figure 3. Emission measurements along the SiC filament.

3. Results

Figure 4 shows laser-backlit and flame images of the ethanol droplets burning in the O_2/N_2 and O_2/CO_2 environments (which were captured 0.5 s after ignition). For all of the experiments performed, the initial droplet diameter (of 1.8 ± 0.1 mm) was kept constant and the O_2 concentration was elevated from 30% to 50% at 0.24 MPa. A soot shell of

varying opacity (which indicates the magnitude of the sooting propensity) formed around the ethanol droplet represented by a black solid circle in the laser-backlit images. The ethanol droplets burned in the 30% and the 40% O_2 concentrations produced a distinct soot shell with variations in the magnitude of the sooting propensity with time. It was also observed that the soot shell that formed in the 50% O_2 concentration quickly vanished after ignition. Increasing the O_2 concentration caused changes in flame luminosity over time, owing to variations in the thermal radiation emitted by the soot particles and the gases.

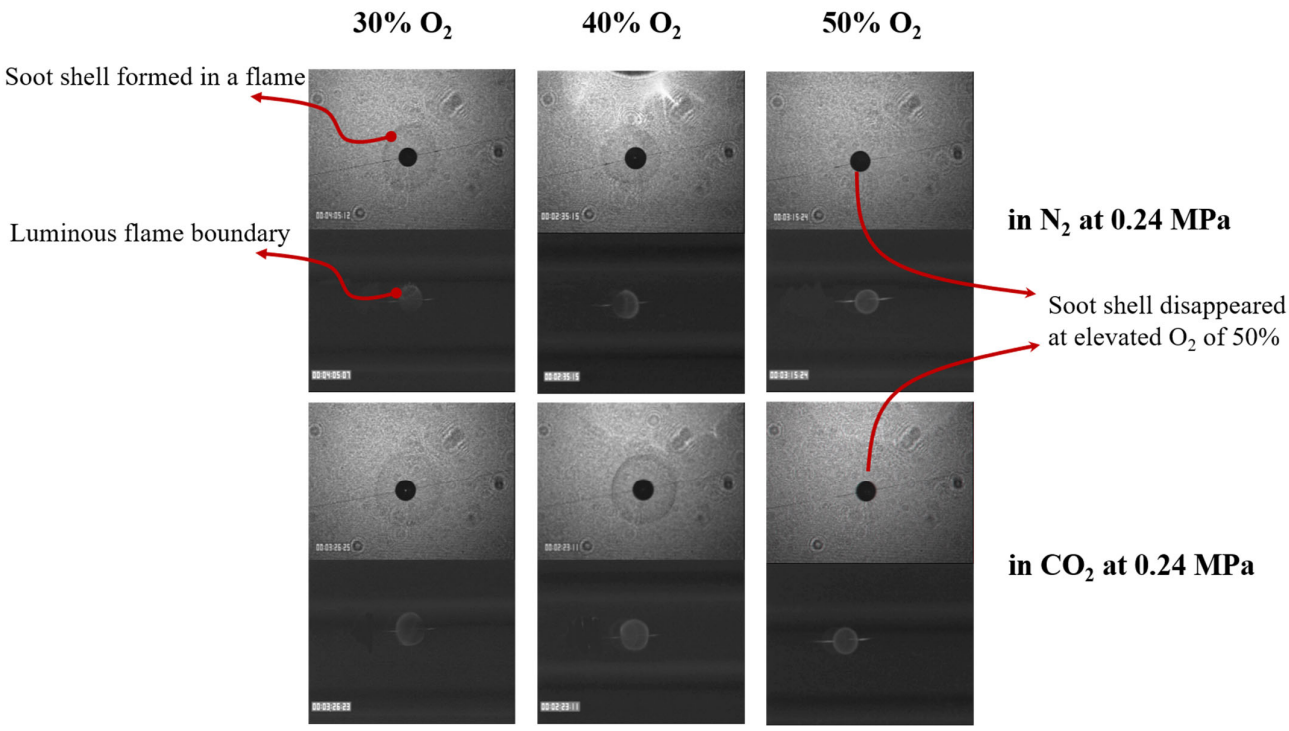

Figure 4. Laser-backlit and flame images of ethanol droplets burning in O_2/N_2 and O_2/CO_2 environments.

Figure 5 displays the results of the analysis of the droplet and flame histories of the ethanol droplets burning in 40% O_2 in the N_2 and CO_2 environments. In Figure 5a, a linear fit to the evolution of the square of the droplet diameter d^2 over time after the transient heat-up period yielded the droplet burning rate K. The flame standoff ratio (FSR) computed by dividing the flame diameter by the instantaneous droplet diameter increased initially and then approached quasi-steady behavior over time. The measured droplet burning rates K and average FSRs (determined from the quasi-steady state) for the experiments in Figure 4 were plotted as a function of O_2 concentration, as shown in Figure 5b.

In all of the experiments performed at O_2 concentrations ranging from 30% to 50%, the burning rates in the N_2 environments were higher than in the corresponding O_2 concentrations in the CO_2 environments. The lowered burning rate of ethanol in the CO_2 environments is primarily due to the higher heat capacity of CO_2 in comparison to N_2 (see Figure 6; data obtained from the NIST Chemistry WebBook, SRD 69 [26]). Previous investigations [21] have clearly demonstrated that the increased heat losses caused through the radiative emission from the flame can influence the burning behavior of microgravity droplet flames. The radiative emission is proportional to the volume of the soot-containing flame which varies with inert substitution. In particular, the larger flame diameter in the CO_2 environments represents a larger volume of the radiatively participating medium comprising soot and gases such as CO_2 and H_2O which can result in higher heat losses from the flame and thus lower the droplet burning rate. However, as will be discussed later in Figure 7, the measured radiative heat losses were slightly higher in the N_2 environment as compared with the CO_2 environment. This result implies that the reduction in the burning

rate caused through the presence of the CO_2 around the droplet is solely attributable to the high specific heat of the CO_2 rather than the influence of radiative heat loss. Furthermore, the differences in heat capacity and flame volume do not fully explain why the burning rate of ethanol droplets in the N_2 environments increased non-linearly in the O_2 environments but linearly in the CO_2 environments.

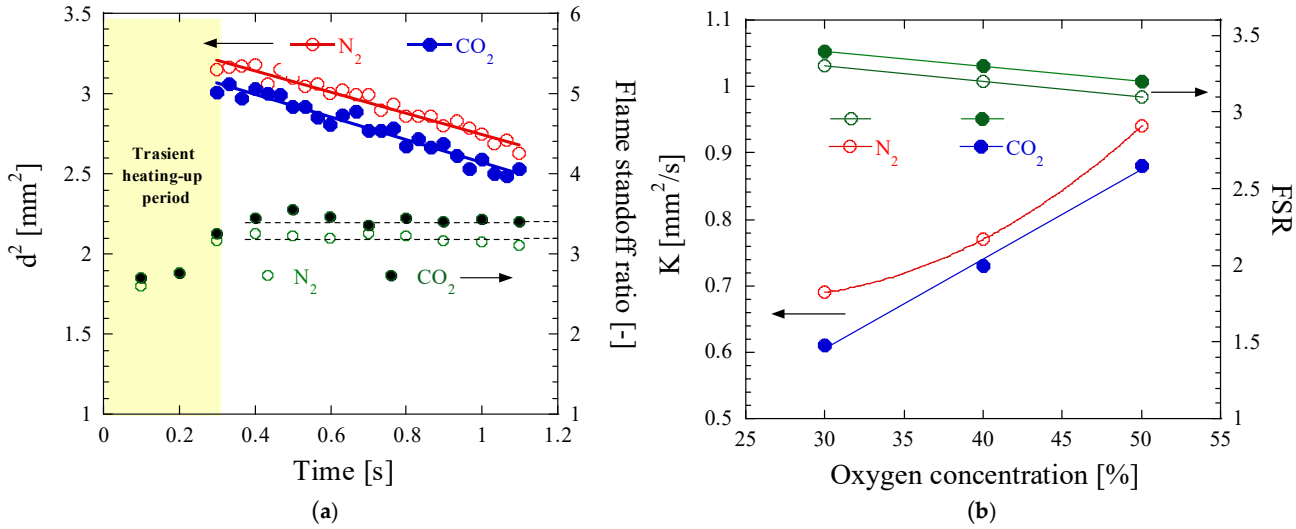

Figure 5. Droplet burning and flame histories in O_2/N_2 and O_2/CO_2 environments: (**a**) measured square of the droplet diameter and FSR as a function of time; (**b**) droplet burning rate and flame standoff ratio versus O_2 concentration.

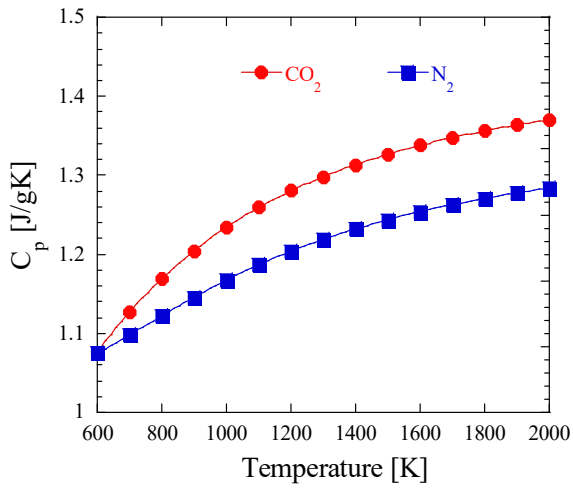

Figure 6. Heat capacity for CO_2 and N_2 as a function of temperature.

To better understand the impact of radiative heat losses on burning behavior, the radiative heat loss fraction was calculated as follows:

$$X_r = \frac{Q_m}{Q_c} \tag{1}$$

where Q_m is the measured radiative emission power (mW) and Q_c is the rate of heat generation (mW). For each of the experiments performed, Q_c was calculated using the following equation:

$$Q_c = \frac{\pi \rho_l K \Delta H d}{4} \tag{2}$$

where ρ_l is the liquid density of the fuel (g/mm^3), K is the average burning rate constant (mm^2/s), ΔH is the heat of combustion per unit of mass of the fuel (J/g), and d is the droplet diameter (mm).

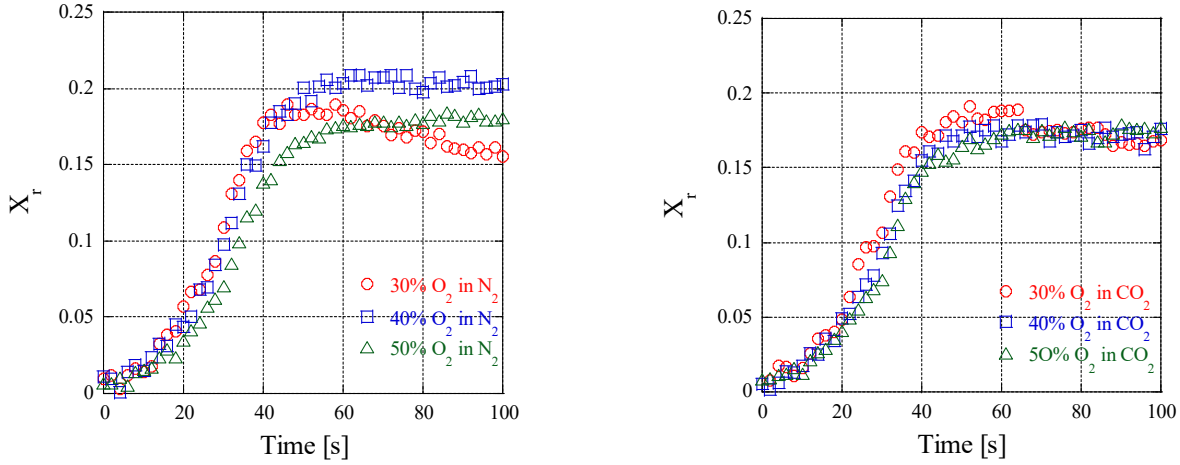

(**a**) Ethanol droplets burning in O_2/N_2 environments (**b**) Ethanol droplets burning in O_2/CO_2 environments

Figure 7. Radiative heat loss fraction in O_2/N_2 and O_2/CO_2 environments as a function of time.

Figure 7a,b shows the calculated radiative heat loss fractions as a function of time when the O_2 concentrations in the N_2 and the CO_2 environments vary from 30% to 50%. As shown in the figures, the radiative heat loss fraction rapidly increases and approaches the quasi-steady values in all of the experiments. The most dramatic change in radiative heat loss fractions with the O_2 concentrations happens in the N_2 environments. In the CO_2 environments, however, the increases in the O_2 concentrations have relatively little effect on the radiative heat loss fraction compared to in the N_2 environments. Interestingly, the radiative heat loss fraction observed in the N_2 environments increases as the O_2 concentration increases from 30% to 40% but falls drastically when the O_2 concentration reaches 50%. These intriguing phenomena are closely related to sooting behaviors along with the flame temperature variations. Since soot forms through pyrolysis reactions with a high activation energy [22], the sooting behavior in diffusion flames is sensitive to changes in flame temperature. In an effort to quantitatively investigate the sooting behavior of ethanol droplet flames, the measured maximum flame temperatures $T_{f\,max}$ and soot-volume fractions $f_{v\,max}$ were summarized, as shown in Table 1. For each experiment, the $f_{v\,max}$ and the $T_{f\,max}$ were determined from the time-varying distributions of the soot-volume fraction and the flame temperature measurements. The range of the $T_{f\,max}$ for the N_2 varied from 1780 K to 2217 K, and for the CO_2, from 1710 K to 2165 K, as the O_2 concentration in the ambient atmosphere increases. The higher $T_{f\,max}$ of the ethanol droplet flames in the N_2 environments was primarily due to the higher heat capacity of CO_2 with respect to N_2. Based on the differences in the heat capacity, the presence of CO_2 around the flame produced a lower $T_{f\,max}$, which was approximately 50 ~ 100 K lower than that of N_2. The measured $f_{v\,max}$ ranges from 3.5 ppm for the 40% O_2 concentration in the N_2 environment (the lowest value) to 4.4 ppm for the 30% O_2 concentration in the CO_2 environment (the highest value). Despite the slightly lower flame temperatures in the CO_2 environment compared to the N_2 environment, the CO_2 environment exhibited similar sooting behavior to that seen in the N_2 environment (in terms of $f_{v\,max}$ measured as a function of O_2) due to the longer residence time of fuel vapor (τ_r), as shown in Table 1. The longer the residence time of the fuel molecules in a high-temperature environment, the greater the potential for sooting enabled through fuel pyrolysis, nucleation, and surface growth [22]. In this study, the residence time of the fuel vapor within the region bounded by means of the droplet surface and the flame front was calculated using the formulation suggested in the authors' previous works (see Appendix A for more details).

Table 1. Summary of measured $T_{f\,max}$, τ_r, and $f_{v\,max}$ for all experimental conditions.

Ambient		$T_{f\,max}$ [K]	τ_r [ms]	$f_{v\,max}$ [ppm]
30% O_2	in N_2	1780	69	4.2
	in CO_2	1710	86	4.1
40% O_2	in N_2	1994	48	3.5
	in CO_2	1891	63	4.4
50% O_2	in N_2	2217	31	-
	in CO_2	2165	40	-

Figure 8 displays the measured $f_{v\,max}$ plotted with respect to the inverse of $T_{f\,max}$. The measured $f_{v\,max}$ initially increased, reached a maximum, and then promptly decreased with the increasing O_2 concentrations in both the N_2 and the CO_2 environments, as shown in the figure. These interesting non-monotonic behaviors of $f_{v\,max}$ with the increased O_2 concentrations are linked to the competition between the pyrolysis reactions leading to the soot precursors and the onset of fragmentation of the formed soot precursors influenced by the temperature, as well as the oxidation of the soot precursors and the particles [22]. Because the pyrolysis reactions are rate-controlling at lower temperatures, the $f_{v\,max}$ increased with temperature. As the temperature increased beyond the threshold value, however, the formed soot precursors fragmented due to the decrease in their thermodynamic stability, thereby reducing the soot yield. As the O_2 concentration in the ambient environment is elevated, there is also expected to be greater degrees of leakage of OH radicals across the flame front towards the fuel-rich region which can enhance the oxidation of the soot precursors and the soot particles [22]

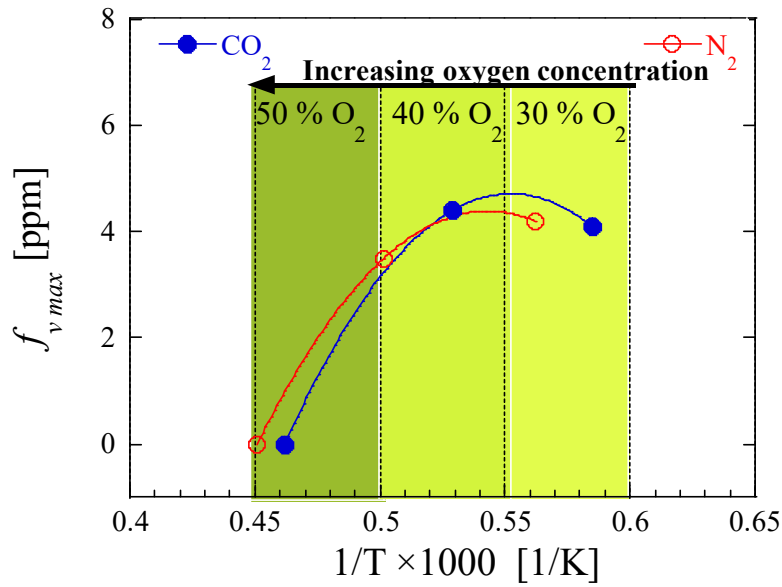

Figure 8. Measured $f_{v\,max}$ with respect to the inverse of $T_{f\,max}$.

More importantly, the non-monotonic behaviors of $f_{v\,max}$ appeared to have a significant impact on variations in the magnitude of radiative heat loss in the N_2 environment with the increased O_2. Despite reductions in the $f_{v\,max}$ from the increasing O_2 concentration from 30% to 40%, the magnitude of the radiative emissions from the soot particles increased due to the comparatively high flame temperature, as shown in Figure 6a. However, the magnitude of the radiative emissions was reduced through increasing the O_2 concentration up to 50% regardless of the flame temperature, as the soot particles disappeared within the flame. In contrast to the N_2 environment, the magnitude of the radiative emissions in the CO_2 environments was nearly identical despite the non-monotonic $f_{v\,max}$ behaviors

produced through the increasing O_2. Because CO_2 (which is not convected away due to the lack of buoyant flow) is a radiatively participating gas, it absorbed radiative energy from the flame and thus increased the temperatures of the surrounding gases. As a result, the CO_2 around the flame in microgravity provides an increased optical thickness, compared to in normal gravity, eventually blocking radiation emissions from the flame to the surroundings.

4. Conclusions

Experiments were performed to investigate the influence of the presence of CO_2 around a single ethanol droplet flame on burning behavior and radiative properties in microgravity. The experimental data show that ethanol droplets burning in N_2 environments produced a higher droplet burning rate than in the CO_2 environments due to the lower heat capacity of N_2. The non-monotonic sooting behaviors resulting from an increase in flame temperatures (by means of the elevated O_2 concentrations) were found to effectively influence the radiative heat losses in the N_2 environments, eventually leading to non-linear droplet burning behaviors with the O_2 concentrations. However, the radiative heat losses from the flame to the surroundings in the CO_2 environments were suppressed irrespective of the non-monotonic sooting behaviors. It is believed that the CO_2, as a radiatively participating gas, was not convected away due to the lack of buoyant flow and hence absorbed radiative energy from the flame, raising the temperatures of the surrounding gases. The findings obtained from this study can contribute to a better understanding of the complex physics of CO_2 gas radiation in microgravity and help to develop more effective fire suppression systems for human spacecraft and interplanetary habitats.

Author Contributions: S.-H.P. provided the main idea of the study; T.-K.H. designed and performed the experiments; T.-K.H. wrote the original draft; S.-H.P. reviewed and edited the drafts. All authors have read and agreed to the published version of the manuscript.

Funding: This work was supported by the Korea Institute of Energy Technology Evaluation and Planning (KETEP) and the Ministry of Trade, Industry & Energy (MOTIE) of the Republic of Korea (No. 20215810100040) and by a Korea Agency for Infrastructure Technology Advancement (KAIA) grant funded by the Ministry of Land, Infrastructure and Transport (Grant RS-2022-00156237).

Institutional Review Board Statement: Not applicable.

Informed Consent Statement: Not applicable.

Data Availability Statement: Data are contained within the article.

Conflicts of Interest: The authors declare no conflict of interest. The funders had no role in the design of the study; in the collection, analysis, or interpretation of data; in the writing of the manuscript; or in the decision to publish the results.

Appendix A

In particular, variations in flame temperature as well as heat and species transport characteristics are important factors to consider when interpreting the sooting behavior of droplet flames in microgravity [22]. The heat and species transport characteristics of microgravity droplet flames can be represented by the residence time of fuel vapor transport, which defines the duration of the pyrolysis reactions leading to the species required for PAH formation, soot nucleation, and surface growth [22].

By integrating the inverse of the radial gas velocity, *U(r)*, the residence time τ_r of the fuel vapor transport in the spherically symmetric flame geometry shown in Figure A1 can be calculated as:

$$\tau_r = \int_{r_d}^{r_f} \frac{1}{U(r)} dr \tag{A1}$$

where r_d and r_f indicate the droplet surface and flame front, respectively. The radial velocity U is the sum of the Stefan velocity Vs and the fuel mass diffusion velocity V_F. The Stefan and fuel mass diffusion velocities are expressed as:

$$V_S = \frac{K\rho_l r_d}{8\rho_g r^2} \tag{A2}$$

$$V_F = -D\frac{ln(1 - Y_{F.S})(1 - Y_{F.S})r_d}{r^2} \tag{A3}$$

where ρ_l is the liquid-phase density, ρ_g is the gas-phase density, D is the mass diffusion coefficient of the fuel in the gas phase, and $Y_{F.S}$ is the droplet surface mass fraction. In this study, D was calculated using the Chapman–Enskog theoretical model (Reid et al., 1987) [27]:

$$D = \frac{0.0266T^{\frac{3}{2}}}{PMW^{\frac{1}{2}}\sigma^2\Omega_D} \tag{A4}$$

where P is the atmospheric pressure, MW represents the molecular weights of species, σ represents the hard-sphere collision diameters, and Ω_D represents the collision integral.

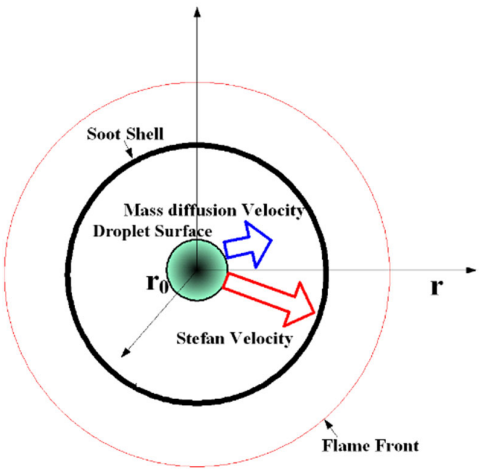

Figure A1. One-dimensional spherically symmetric flame geometry.

In Figure A2, the calculated Stefan and fuel mass diffusion velocities were plotted as a function of the normalized radial location (r/r_d) of the ethanol droplets burning in the O_2/N_2 and O_2/CO_2 environments. The Stefan and fuel mass diffusion velocities were found to increase to a maximum at the droplet surface and subsequently decrease with radial position. The largest temperature gradients occur near the droplet surface (at $r/r_d = 1$), resulting in higher Stefan velocities (due to a rapid reduction in the gas-phase density) and fuel mass diffusion velocities (due to increased mass diffusivities). After reaching the maximum value, the Stefan and fuel mass diffusion velocities drop due to the increased relevance of the squared radius factor in the denominator of Equtaion (2) and (3) (Choi, 1993) [21]. As shown in Figure A2, the magnitude of the Stefan velocities is significantly larger in comparison to that of the fuel mass diffusion velocities in all of the environments. These experimental results imply that the calculation of the residence time of the fuel vapor transport is strongly influenced mainly by means of the Stefan velocities relative to the fuel mass diffusion velocities. However, the mass diffusion velocities become prominent as the O_2 concentration increases, since the mass diffusion coefficient D of fuel in the gas phase is proportional to $T^{3/2}$. Furthermore, the maximum values of both the Stefan and fuel mass diffusion velocities in the O_2/N_2 environments are higher than the values calculated in the O_2/CO_2 environments due to higher droplet burning rates and mass diffusivity.

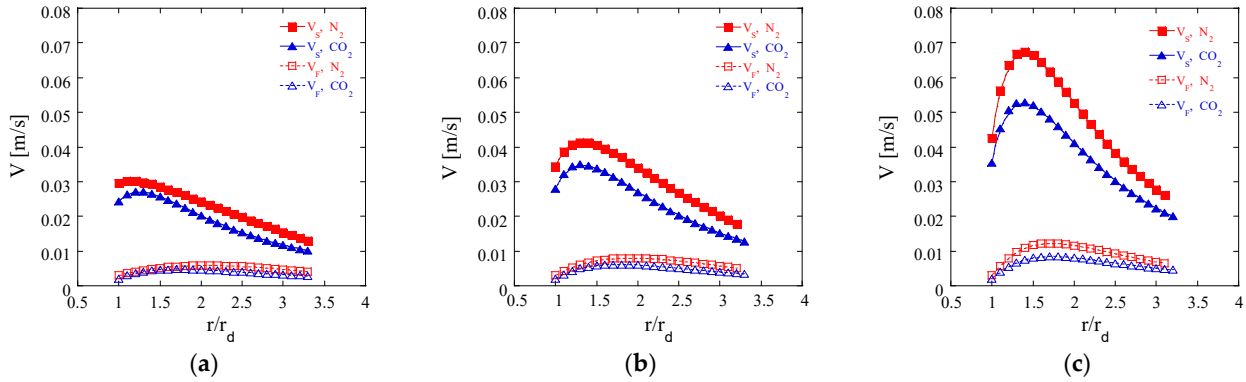

Figure A2. Stefan and fuel mass diffusion velocities plotted versus non-dimensionalized flame locations. (**a**) Ethanol droplets burning in 30% O_2 in N_2 and CO_2 environments. (**b**) Ethanol droplets burning in 40% O_2 in N_2 and CO_2 environments. (**c**) Ethanol droplets burning in 50% O_2 in N_2 and CO_2 environments.

References

1. Kauffman, J. Adding Fuel to the Fire: NASA's Crisis Communications Regarding Apollo 1. *Public Relat. Rev.* **1999**, *25*, 421–432. [CrossRef]
2. Ruff, G.A.; Urban, D.L.; King, M.K. A Research Plan for Fire Prevention Detection and Suppression, AIAA-2005-0341. In Proceedings of the 43rd Aerospace Sciences Meeting and Exhibit, Reno, NV, USA, 9–12 January 2005. [CrossRef]
3. Urban, D.L.; Ruff, G.A.; Brooker, J.; Cleary, T.; Yang, J.C.; Mulholland, G.W.; Yuan, Z.G. Spacecraft Fire Detection: Smoke Properties and Transport in Low-Gravity. In Proceedings of the 46th AIAA Aerospace Sciences Meeting and Exhibit, Reno, NV, USA, 7–10 January 2008.
4. Brooker, J.E.; Urban, D.L.; Ruff, G.A. ISS Destiny Laboratory Smoke Detection Model. In Proceedings of the 37th International Conference on Environmental Systems (ICES), Chicago, IL, USA, 9–12 July 2007. [CrossRef]
5. Hong, T.K.; Park, S.-H. Numerical Analysis of Smoke Behavior and Detection of Solid Combustible Fire Developed in Manned Exploration Module Based on Exploration Gravity. *Fire* **2021**, *4*, 85. [CrossRef]
6. Hicks, M.C.; Nayagam, V.; Williams, F.A. Microgravity droplet combustion in CO_2 enriched environments at elevated pressures. In Proceedings of the 5th US Combustion Meeting, San Diego, CA, USA, 25–28 March 2007.
7. Hicks, M.C. *Microgravity Droplet Combustion in Carbon Dioxide Enriched Environments*; Case Western Reserve University Press: Cleveland, OH, USA, 2016.
8. Son, Y.; Zouein, G.; Gokoglu, S.; Ronney, P.D. Comparison of Carbon Dioxide and Helium as Fire Extinguishing Agents for Spacecraft. *J. ASTM Int.* **2006**, *3*, 253–361. [CrossRef]
9. Katta, V.R.; Takahashi, F.; Linteris, G.T. Suppression of Cup-Burner Flames Using Carbon Dioxide in Microgravity. *Combust. Flame* **2004**, *137*, 506–522. [CrossRef]
10. Godsave, G.A.E. Burning of fuel droplets. *Nature* **1950**, *166*, 1111. [CrossRef]
11. Jackson, G.; Avedisian, C.; Yang, J. Observations of Soot During Droplet Combustion at Low Gravity: Heptane and Heptane/Monochloroalkane Mixtures. *Int. J. Heat Mass Transf.* **1992**, *35*, 2017–2033. [CrossRef]
12. Nakaya, S.; Fujishima, K.; Tsue, M.; Kono, M.; Segawa, D. Effects of Droplet Diameter on Instantaneous Burning Rate of Isolated Fuel Droplets in Argon-rich or Carbon Dioxide-rich Ambiences under Microgravity. *Proc. Combust. Inst.* **2013**, *34*, 1601–1608. [CrossRef]
13. Dietrich, D.L.; Nayagam, V.; Hicks, M.C.; Ferkul, P.V.; Dryer, F.L.; Farouk, T.; Shaw, B.D.; Suh, H.K.; Choi, M.Y.; Williams, F.A. Droplet Combustion Experiments Aboard the International Space Station. *Microgravity Sci. Technol.* **2014**, *26*, 65–76. [CrossRef]
14. Hicks, M.C.; Nayagam, V.; Williams, F.A. Methanol Droplet Extinction in Carbon-Dioxide-Enriched Environments in Microgravity. *Combust. Flame* **2010**, *157*, 1439–1445. [CrossRef]
15. Farouk, T.I.; Dryer, F.L. On the Extinction Characteristics of Alcohol Droplet Combustion under Microgravity Conditions—A Numerical Study. *Combust. Flame* **2012**, *159*, 3208–3223. [CrossRef]
16. Farouk, T.I.; Dryer, F.L. Tethered Methanol Droplet Combustion in Carbon-dioxide Enriched Environment under Microgravity Conditions. *Combust. Flame* **2012**, *159*, 200–209. [CrossRef]
17. Nayagam, V.; Dietrich, D.L.; Hicks, M.C.; Williams, F. A Radiative Extinction of Large n-Alkane Droplets in Oxygen-Inert Mixtures in Microgravity. *Combust. Flame* **2018**, *194*, 107–114. [CrossRef]
18. Manzello, S.L.; Park, S.H.; Yozgatligil, A.; Choi, M.Y. Fuel-dependent Effects on Droplet Burning and Sooting Behaviors in Microgravity. *Energy Fuels* **2009**, *23*, 3586–3591. [CrossRef]
19. Yozgatligil, A.; Park, S.H.; Choi, M.Y. Burning and Sooting Behavior of Ethanol Droplet Combustion under Microgravity Conditions. *Combust. Sci. Technol.* **2004**, *176*, 1985–1999. [CrossRef]

20. Nayagam, V.; Haggard, J.B.; Colantonio, R.O.; Marchese, A.J.; Dryer, F.L.; Zhang, B.L.; Williams, F.A. Microgravity n-Heptane Droplet Combustion in Oxygen-Helium Mixtures at Atmospheric Pressure. *AIAA J.* **1998**, *36*, 1369–1378. [CrossRef]
21. Choi, M.Y.; Dryer, F.L.; Green, G.J.; Sangiovanni, J.J. Soot Agglomeration in Isolated, Free Droplet Combustion. In Proceedings of the 31st Aerospace Sciences Meeting, Reno, NV, USA, 11–14 January 1993. [CrossRef]
22. Park., S.H. Investigation of Sooting Behavior and Soot Nanostructures of Ethanol Droplet Flames in Microgravity. Ph.D. Thesis, Drexel University, Philadelphia, PA, USA, 2007.
23. Dasch, C.J. One-Dimensional Tomography: A Comparison of Abel, Onion-Peeling, and Filtered Backprojection Methods. *Appl. Opt.* **1992**, *31*, 1146–1152. [CrossRef] [PubMed]
24. Vilimpoc, V.; Goss, L. SiC-based Thin-Filament Pyrometry: Theory and Thermal Properties. *Int. Symp. Combust.* **1989**, *22*, 1907–1914. [CrossRef]
25. Bundy, M.; Hamins, A.; Lee, K.Y. Suppression Limits of Low Strain Rate Non-Premixed Methane Flames. *Combust. Flame* **2003**, *133*, 299–310. [CrossRef]
26. NIST. NIST Chemistry WebBook: Nist Standard Reference Database Number 69. Available online: https://webbook.nist.gov/chemistry/ (accessed on 22 November 2023).
27. Reid, R.C.; Prausnitz, J.M.; Poling, B.E. *The Properties of Gases and Liquids*, 4th ed.; McGraw Hill, Government Printing Office: New York, NY, USA, 1987.